0.532-μm laser conditioning of HfO_2/SiO_2 third harmonic separator fabricated by electron-beam evaporation

Dawei Li (李大伟)[1,2], Yuan'an Zhao (赵元安)[1], Jianda Shao (邵建达)[1], Zhengxiu Fan (范正修)[1], and Hongbo He (贺洪波)[1]

[1]*Shanghai Institute of Optics and Fine Mechanics, Chinese Academy of Sciences, Shanghai 201800*
[2]*Graduate University of Chinese Academy of Sciences, Beijing 100049*

Received October 9, 2007

The 0.532-μm laser conditioning of HfO_2/SiO_2 third harmonic separator fabricated by electron-beam evaporation (EBE) was studied. The laser induced damage threshold (LIDT) of the separator determined by 1-on-1 test is 9.1 J/cm^2 and it is 15.2 J/cm^2 after laser conditioning determined by raster scanning. Two kinds of damage morphologies, taper pits and flat bottom pits, are found on the sample surface and they show different damage behaviors. The damage onset of taper pits does not change obviously and the laser conditioning effect is contributed to the flat bottom pits, which limits the application of laser conditioning.

OCIS codes: 140.3330, 310.6870.

A significant limitation on operating fluence of high peak power lasers is laser induced damage threshold (LIDT) of optical thin films. In laser systems with frequency conversion, multiple wavelengths will be present on some optical components, such as harmonic separators and third harmonic separators, so these components are susceptible to damage especially. In recent years some methods have been presented to enhance the laser resistance of optical films, and one of them is laser conditioning[1−4]. Although many experiment results have been reported and a number of mechanisms[5−9] have been proposed as being responsible for the observed laser conditioning effect, we are still lack of a complete physical explanation for it. To understand the laser conditioning effect on HfO_2/SiO_2 separator and enhance its laser resistance capability better, this letter investigated the 0.532-μm laser conditioning of HfO_2/SiO_2 third harmonic separator prepared by electron-beam evaporation (EBE).

The samples were prepared by EBE on K9 glass substrates and the coating design was $HL(H2L)^{15}$, where H denoted high index material HfO_2 with one quarter-wavelength optical thickness (QWOT) and L denoted low index material SiO_2 with one QWOT.

The experimental setup was built according to ISO-11254[10,11] as shown schematically in Fig. 1. The Nd:YAG laser system outputted pulses at 0.532 μm with pulse-width of 10 ns. The laser beam was focused on the target plane normally with Gaussian diameter ($1/e^2$) of 0.5 mm by a non-spherical lens of 400-mm focal length. The attenuator comprised of a half wavelength plate and a polarizer was employed to adjust the pulse energy irradiating the sample. The sample was mounted normal to the beam in a step motor, which was used to position different test sites. The online imaging system of 200× magnifications comprised of microscope and charge-coupled device (CCD) was used to observe the test area and check whether the damage occurred. Damage was defined as any visual change in the sample after laser irradiation.

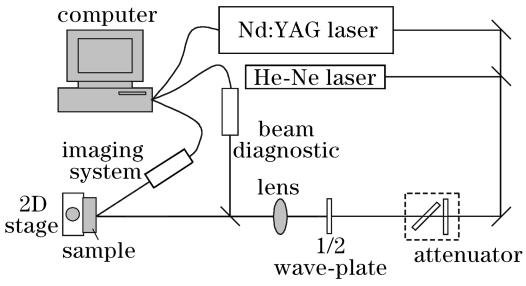

Fig. 1. Experimental setup for damage and laser conditioning.

1-on-1 damage test[10] was done firstly. Twenty sites on the sample surface were exposed to the same pulse energy and the fraction of damage was recorded. The procedure was repeated for different pulse energies until it was sufficiently broad to include points of both zero and 100% damage probabilities. The damage data were linearly extrapolated to the zero damage probability and the LIDT was obtained as 9.1 J/cm^2.

Laser conditioning was conducted by raster scanning which had been described by Sheehan[12] *et al.*. In summary, the sample was translated past a stationary laser beam to raster scan the entire surface of the sample. By defining the step size between pulses to equal the laser beam diameter at 90% of the peak energy density, the entire surface was exposed to the 90% peak laser energy density. In the next scanning the pulse energy was enhanced. Here the starting pulse energy density was 20% of the 1-on-1 LIDT, and the increment is 10% of it, which is shown in Fig. 2. During raster scanning, the laser pulse energy density was 15.2 J/cm^2 when damage occurred.

There were two damage morphologies found on the sample surface after damage test and raster scanning. Atomic force microscopy (AFM) images are shown in Fig. 3. One of them was taper pit as Fig. 3(a) with about 5-μm diameter at the sample surface and depth varying from 0.4 to 1.1 μm. The other one was flat bottom pit

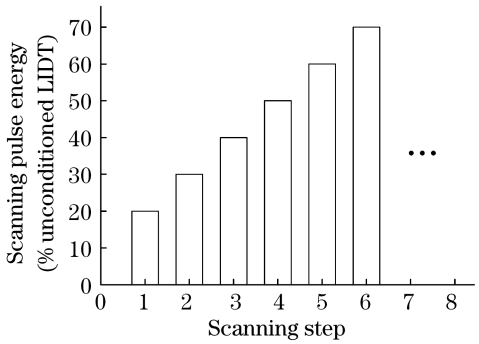

Fig. 2. n-step raster scanning.

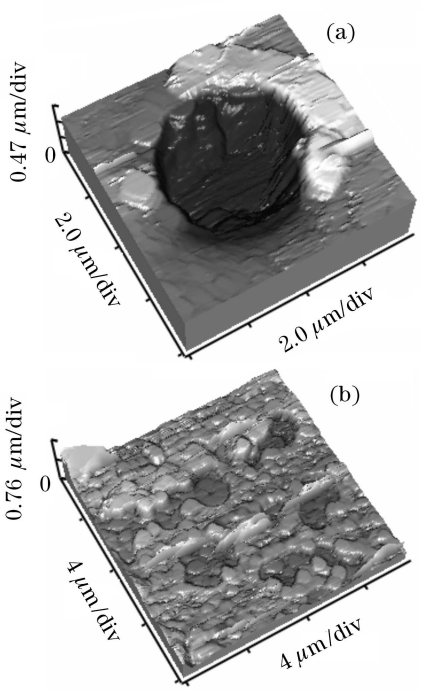

Fig. 3. AFM micrographs of damage morphologies. (a) Taper pits; (b) flat bottom pits.

as shown in Fig. 3(b). They had a typical cylindrical shape with diameter about 3 μm and depth about 0.2 μm. Generally there were several such pits linked together. In a lot of cases, a small melted zone was obvious at the center of the damage.

The formation of taper pits was studied and it was thought to be caused by nodular defects[13−15]. The nodular defects formed during film deposition were unstable and during laser pulse irradiation they were heated until ejection and taper pits were formed finally. From the experiments, the results show that the pulse energy density is 15.2 J/cm^2 for both the 1-on-1 test and raster scanning when taper pits emerges, so the damage onset of the nodular defects does not change obviously after raster scanning. As to the flat bottom pits, Dijon[16] thought that they were initiated by some invisible absorbing centers and he proposed four steps leading to the flat bottom pits:

1) The small center strongly absorbs the light and reaches a very high temperature. The heat deposited in the inclusion allows to melt a tiny cavity around the center.

2) With the irradiation of laser pulse, the cavity gets hotter and hotter and radiates ultraviolet energy which is linearly absorbed by the materials around the cavity and allows injection of electrons.

3) The electrons in the materials are strongly absorbing and transfer part of the energy to the lattice which could heat the film to a temperature higher than the melting point.

4) The flat bottom pit is formed after the buckling of the outer layers due to the thermomechanical effect.

In 1-on-1 test the flat bottom pits appeared when the pulse energy density was 9.1 J/cm^2. But during raster scanning we found them only when the pulse energy density was more than 16.0 J/cm^2. This suggests that raster scanning enhances the laser resistance capability of this kind of defect.

In summary, two kinds of damage morphologies, taper pit and flat bottom pit, are found on the surface of HfO_2/SiO_2 third harmonic separator and they are thought to be initiated by nodular defects and absorbing centers respectively. Laser conditioning effect is observed for the absorbing centers, but the LIDT of the nodular defects does not change obviously after raster scanning, which limits the application of laser conditioning.

D. Li's e-mail address is dawei_510@yahoo.com.cn.

References

1. C. J. Stolz, L. M. Sheehan, S. M. Maricle, S. Schwartz, and J. Hue, Proc. SPIE **3578,** 55 (1999).
2. A. F. Stewart, L. Bonsall, J. R. Bettis, J. Copland, K. P. Healey, G. B. Charlton, W. Hughes, and J. C. Echeverry, Proc. SPIE **3578,** 39 (1999).
3. M. R. Kozlowski, C. R. Wolfe, M. C. Staggs, and J. H. Campbell, Proc. SPIE **1438,** 376 (1989).
4. J. Huang, H. Lü, B. Ye, S. Zhao, H. Wang, X. Jiang, X. Yuan, and W. Zheng, Chinese J. Lasers **34,** 723 (2007).
5. Y. Cui, Y. Zhao, Y. Jin, Z. Fan, and J. Shao, Acta Opt. Sin. **27,** 1129 (2007).
6. C. R. Wolfe, M. R. Kozlowski, J. H. Campbell, F. Rainer, A. J. Morgan, and R. P. Gonzales, Proc. SPIE **1438,** 360 (1989).
7. J. W. Arenberg and M. E. Frink, Proc. SPIE **756,** 430 (1988).
8. J. W. Arenberg and D. W. Mordaunt, Proc. SPIE **775,** 516 (1989).
9. N. J. Hess, G. J. Exarhos, and M. J. Iedema, Proc. SPIE **1848,** 243 (1993).
10. ISO 11254-1, Lasers and laser-related equipment-Determination of laser-induced damage threshold of optical surfaces — Part 1: 1-on-1 test (2002).
11. Y. Zhao, T. Wang, D. Zhang, J. Shao, and Z. Fan, Appl. Surf. Sci. **245,** 335 (2005).
12. L. Sheehan, M. Kozlowski, F. Rainer, and M. Staggs, Proc. SPIE **2114,** 559 (1994).
13. B. Liao, D. J. Smith, and B. Mcintyre, Proc. SPIE **746,** 305 (1987).
14. K. Lewis, G. Smith, and A. Pidduck, Proc. SPIE **4932,** 26 (2003).
15. C. J. Stolz, F. Y. Genin, and T. V. Pistor, Proc. SPIE **5273,** 41 (2004).
16. J. Dijon, G. Ravel, and B. André, Proc. SPIE **3578,** 31 (1999).